PCCP

PAPER

View Article Online
View Journal | View Issue

Cite this: *Phys. Chem. Chem. Phys.*, 2023, **25**, 5262

Vibrational spectroscopy of $Cu^+(H_2)_4$: about anharmonicity and fluxionality†

Jiaye Jin, [a] Toshiki Wulf, [abc] Marcel Jorewitz, [a] Thomas Heine *[bc] and Knut R. Asmis *[a]

Received 12th December 2022,
Accepted 24th January 2023

DOI: 10.1039/d2cp05802b

rsc.li/pccp

The vibrational spectra of the copper(I) cation–dihydrogen complexes $Cu^+(H_2)_4$, $Cu^+(D_2)_4$ and $Cu^+(D_2)_3H_2$ are studied using cryogenic ion trap vibrational spectroscopy in combination with quantum chemical calculations. The infrared photodissociation (IRPD) spectra (2500–7300 cm^{-1}) are assigned based on a comparison to IR spectra calculated using vibrational second-order perturbation theory (VPT2). The IRPD spectra exhibit ≈60 cm^{-1} broad bands that lack rotational resolution, indicative of rather floppy complexes even at an ion trap temperature of 10 K. The observed vibrational features are assigned to the excitations of dihydrogen stretching fundamentals, combination bands of these fundamentals with low energy excitations as well as overtone excitations of a minimum-energy structure with C_s symmetry. The three distinct dihydrogen positions present in the structure can interconvert *via* pseudorotations with energy barriers less than 10 cm^{-1}, far below the zero-point vibrational energy. *Ab initio* Born–Oppenheimer molecular dynamics (BOMD) simulations confirm the fluxional behavior of these complexes and yield an upper limit for the timeframe of the pseudorotation on the order of 10 ps. For $Cu^+(D_2)_3H_2$, the H_2 and D_2 loss channels yield different IRPD spectra indicating non-ergodic behavior.

1 Introduction

Transition metal cations do not only play an important role in dihydrogen activation, but also in efficient H_2/D_2 isotope separation. Recently, substantial progress has been made in developing more sustainable isotope separation methods based on selective adsorption from gaseous mixtures in porous materials.[1–5] Two effects are exploited in such materials: (a) heavier H_2 isotopologues are bound more strongly to the metal center due to their lower zero-point energy (ZPE) contribution to the adsorption energy and (b) they also exhibit a smaller effective kinetic radius as a result of their more localized probability density.[5–9] Porous materials containing undercoordinated Cu(I) adsorption sites, *e.g.* Cu(I)-MFU-4*l*, Cu(I)-MOR and Cu(I)-ZSM-5 are found to exhibit superior D_2/H_2 selectivity (>10) also at high temperatures (>77 K).[4,9,10] Understanding the binding of dihydrogen isotopologues to different Cu(I) compounds is therefore important for improving the performance of separation materials. Spectroscopic studies of hydrogen coordination to metal centers in bulk materials typically suffer from structural heterogeneity and hence difficulties in assigning the binding site. This can be avoided by performing experiments on well-defined model compounds isolated in the gas phase using the highly selective and sensitive tool of ion vibrational spectroscopy,[11–14] in particular, in the form of cryogenic ion trap vibrational spectroscopy.[15,16] Another advantage of this approach is that such model compounds are amenable to high-level computational approaches that can be used to benchmark more approximative methods applicable to extended systems.

The copper cation (Cu^+) represents the simplest form of an under-coordinated Cu(I) site. Cu^+–H_2 dissociation energies in $Cu^+(H_2)_n$ complexes have been determined by guided ion beam tandem mass spectrometry.[17] Cu^+ can bind up to four dihydrogen molecules in the first complexation shell. Sequential bond dissociation energies (BDEs) have been obtained from gas phase equilibrium constants for the reactions $Cu^+(H_2)_n \rightarrow Cu^+(H_2)_{n-1} + H_2$, and amount to 64, 70, 37, and 21 kJ mol^{-1} for n = 1–4, respectively.[17] Theory indicates that bonding to molecular hydrogen is largely covalent, consisting mainly of electron donation from the σ orbital of H_2 to the empty Cu^+ 4s orbital and electron backdonation from the filled $3d_{yz}$ (dπ) orbital to the σ* orbital of H_2.[17] Given the filled d-shell electron configuration ($[Ar]3d^{10}$), Cu^+ exhibits pronounced backdonation, which leads to strong binding of H_2 and which can be further enhanced by a surrounding framework.[18]

[a] *Wilhelm-Ostwald-Institut für Physikalische und Theoretisch Chemie, Universität Leipzig, Linnéstr. 2, 04103, Leipzig, Germany. E-mail: knut.asmis@uni-leipzig.de*
[b] *Institute of Resource Ecology, Research Site Leipzig, Helmholtz-Zentrum Dresden-Rossendorf, Permoserstr. 15, 04318, Leipzig, Germany*
[c] *Faculty of Chemistry and Food Chemistry, School of Science, TU Dresden, 01062, Dresden, Germany. E-mail: thomas.heine@tu-dresden.de*

† Electronic supplementary information (ESI) available. See DOI: https://doi.org/10.1039/d2cp05802b

Beyond mass spectrometric studies, vibrational spectroscopy of small metal ion complexes provides insights into their geometric and electronic structure. Infrared photodissociation (IRPD) spectra for non-covalent metal-cation–dihydrogen complexes M^+–H_2/D_2 (M = Li, Na, Al, Cr, Mn, Zn, Ag) have been reported by Bieske and coworkers.[19,20] The rotationally-resolved IRPD spectra indicate that all these cationic complexes adopt a C_{2v} T-shaped M^+–(H_2) geometry rather than the linear M^+–H–H structure that is preferred in the corresponding anion complexes.[20–23] The H–H stretching frequencies are redshifted by 67 cm^{-1} (Na^+–H_2) to 406 cm^{-1} (Ag^+–H_2) relative to the frequency of a free H_2 molecule (4161 cm^{-1}).[24] The extent of the redshift depends on the charge and orbital interactions, which determine the balance between σ donation and π backdonation.[25] The strong bonding in the Cu(I)–H_2 motif is also found in neutral Cu compounds. Correspondingly redshifted IR bands were reported at 3567 cm^{-1} (H_2) and 2582 cm^{-1} (D_2) for the CuH(H_2/D_2) complex in a solid hydrogen matrix.[26] Significant nuclear quadrupole coupling constants in dihydrogen complexes of copper fluoride (CuF) measured by microwave spectroscopy also suggest a strong interaction between the Cu(I) center of CuF and the H_2 molecule.[27] However, the IRPD spectrum of the Cu^+(H_2) complex has not been reported yet, because the Cu^+–H_2 binding energy of 64 kJ mol^{-1} (5375 cm^{-1})[17,28] substantially exceeds the energy of the fundamental transition of the H–H stretching vibration.

The complexes formed by molecular hydrogen and the first-row Σ-state transition metal cations Cr^+, Mn^+, Cu^+, and Zn^+ have been investigated using high-level *ab initio* methods. The calculations identified trends in hydrogen activation, vibrational anharmonicity, and rotational structure along the sequence of four electrostatic complexes covering the range from a relatively floppy van der Waals system ($Mn^+\cdots H_2$) to an almost rigid molecular ion ($Cu^+\cdots H_2$).[28] In this series, the Cu^+ complex is predicted to exhibit the highest binding energy, the smallest anharmonicity and the most red-shifted H_2 stretching vibrational frequency (Cu^+–H_2: 3805 cm^{-1}; Cu^+–D_2: 2691 cm^{-1}).

Here, we report IRPD spectra of the copper–dihydrogen complexes $Cu^+(H_2)_4$, $Cu^+(D_2)_4$, and $Cu^+(D_2)_3H_2$. The IRPD spectra are assigned based on a comparison to IR spectra calculated from second-order vibrational perturbation theory (VPT2) as well as molecular dynamics simulations. Evidence is presented for fast dihydrogen interchange (pseudorotation) that leads to a significant broadening of the vibrational bands.

2 Methods

2.1 Experimental methods

IRPD spectroscopic and mass spectrometric experiments were performed using a cryogenically cooled ion trap triple mass spectrometer described previously.[16,29,30] In brief, Cu^+ cations are transferred to the gas phase from a 10 mM 1 : 4 methanol/water $CuSO_4$ solution (Sigma Aldrich: $CuSO_4$ $5H_2O$, 99%; CH_3OH, 99.9%) using a nanospray ion source. All cations are thermalized to room temperature in a helium-filled radio frequency (RF) ion guide and mass-selected using a quadrupole mass filter. Mass-selected $^{63}Cu^+$ cations are trapped and accumulated in a linear radio-frequency (RF) ring-electrode ion trap filled with ≈1 mbar H_2/D_2 and held at 10 to 14 K. $Cu^+(H_2)_n(D_2)_m$ complexes are formed *via* three body collisions.[31,32] Every 100 ms, all ions are extracted from the trap and transferred into the time-of-flight (TOF) mass spectrometer. They are first extracted and accelerated towards the reflectron stage, separating in time and space according to their mass-to-charge ratios. After reflection, all ions are refocused into the extraction/acceleration region, where the ions of interest are irradiated by a precisely timed infrared laser pulse and subsequently re-accelerated into the linear TOF stage (IR^1MS^2 detection scheme).[30] The IRPD spectra are obtained by irradiating the ions perpendicular to the flight direction with a tunable IR laser pulse generated from an IR optical parametric oscillator/amplifier laser system (LaserVision, OPO/OPA),[33] which is pumped by an unseeded Nd:YAG laser (Continuum Surelite EX). The spectral linewidth of the IR laser radiation is 3.5 cm^{-1}. IRPD spectra are recorded by monitoring the intensity of the irradiated ions and their photofragments simultaneously using a microchannel plate (MCP) detector while continuously scanning the laser wavelength, which is monitored online using a HighFinesse WS6-600 wavelength meter. Typically, three scans were measured and averaged to obtain an IRPD spectrum. The photodissociation cross section σ_{IRPD} is determined as described previously.[16,29]

2.2 Computational methods

Geometry optimizations using the CCSD(T) method[34,35] are performed using the Gaussian 09 D.01 program.[36] The def2-TZVPP basis set,[37] a SuperFine grid (pruned 1 75 974 for H and 2 50 974 for Cu) for the reference calculations and no frozen core, *i.e.* CCSD(T, Full), are used. IR spectra are computed at the minimum-energy geometry using second-order Møller–Plesset perturbation theory (MP2)[38–41] in combination with the def2-TZVPP basis set. The ZPE-corrected BDE D_0 for the reaction $Cu^+(H_2)_4 \rightarrow Cu^+(H_2)_3 + H_2$ is determined using the CCSD(T)/def2-TZVPP electronic energy and the MP2/def2-TZVPP frequencies obtained within the harmonic approximation.

Vibrational frequencies and intensities are also calculated beyond the harmonic approximation using deperturbed vibrational perturbation theory (DVPT2)[42] as implemented in the Gaussian 16 C.01 software.[43] From these, IR spectra are obtained by a 20 cm^{-1} FWHM Gaussian line shape convolution. Rovibrational band profiles are simulated by using the PGopher (10.1) program.[44,45]

Ab initio Born–Oppenheimer molecular dynamics (BOMD) simulations are performed on the MP2/def2-TZVPP potential energy surface using the ORCA program (version 5.0.1)[46,47] with TightSCF convergence criteria (energy change 1×10^{-8}, maximum density change 1×10^{-7}). The time step is set to 0.5 fs and the system is equilibrated at the targeted temperatures using a Berendsen thermostat with the time constants of 10 fs, 30 fs and 100 fs for 1, 3 and 10 k time steps, respectively. After equilibration, the thermostat is turned off and a trajectory of ≥14 k time steps (≥7 ps) is recorded. Vibrational profiles are

obtained *via* Fourier transformation of the dipole moment autocorrelation function and yield the so-called BOMD spectrum. The spectrum is smoothed using Gaussian broadening with a FWHM of 6 cm^{-1} and scaled by a factor of 0.932 to better fit the experimental spectrum to account for the high energy of the vibrational modes relative to the simulation temperature.

3 Results

3.1 TOF mass spectrometry

In order to characterize the stability of Cu^+ complexes with dihydrogen we trapped and accumulated mass-selected $^{63}Cu^+$ cations in the cold ion-trap filled with dihydrogen gas. TOF spectra measured with pure H_2, pure D_2 and a 3 : 1 H_2/D_2 gas mixture in the ion trap are shown in Fig. 1 (see Fig. S1 of the ESI† for additional TOF spectra). The most intense peak in each of the TOF spectra is due to bare $^{63}Cu^+$ cations (parent ions). We observe the formation of $^{63}Cu^+(H_2)_n$ complexes with up to $n = 8$ (Fig. 1a) and $^{63}Cu^+(D_2)_m$ complexes with up to $m = 5$ (Fig. 1b). The complex with four dihydrogen molecules is the most abundant one in all TOF spectra, indicating its high relative stability. Hence, the sequential BDE of the fifth (*vs.* the fourth) dihydrogen molecule in $Cu^+(H_2/D_2)_5$ is found to be considerably smaller, consistent with previous thermochemistry data at higher temperatures (>100 K).[17] For the H_2/D_2 gas mixture the most abundant complex is $Cu^+(D_2)_4$, followed by $Cu^+(D_2)_3H_2$, even though there is three times as much H_2 than D_2 in the gas mixture. The higher probability for D_2 binding is attributed to thermodynamic control resulting from the smaller Cu^+–D_2 (*vs.* Cu^+–H_2) ZPE and hence larger BDE.

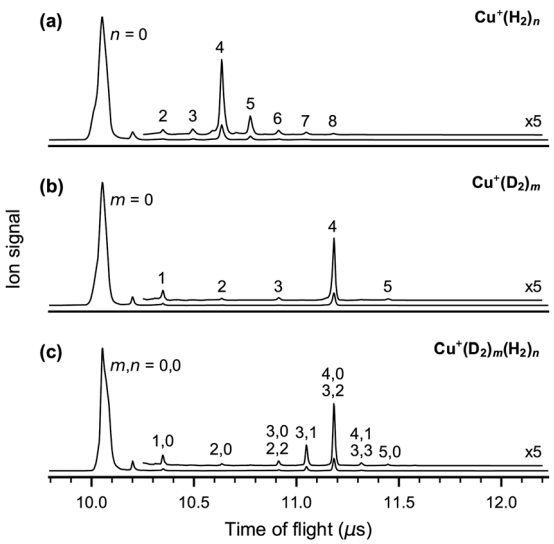

Fig. 1 TOF spectra obtained after trapping and accumulating mass-selected $^{63}Cu^+$ cations in (a) pure H_2 at 10 K, (b) pure D_2 at 14 K, and (c) a 3 : 1 gas mixture of H_2 and D_2 at 10 K. Peaks are assigned to $Cu^+(H_2)_n(D_2)_m$ complexes and labeled accordingly. $^{65}Cu^+$ cations of the naturally slightly less abundant isotope are not fully discriminated against in the quadrupole mass filter and also contribute to the TOF peak at 10.2 μs.

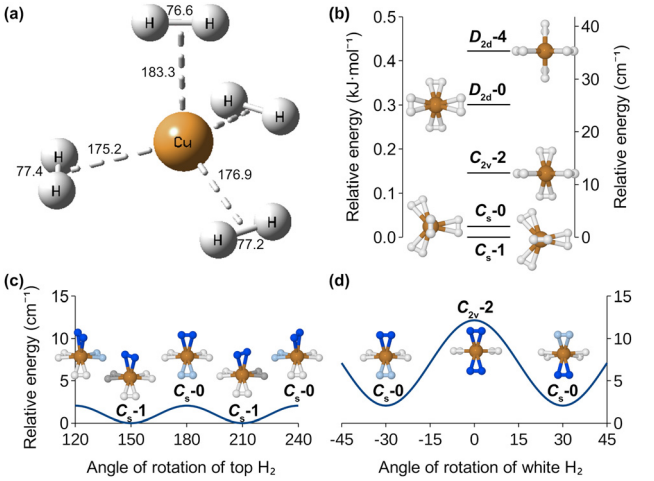

Fig. 2 (a) CCSD(T)/def2-TZVPP minimum-energy structure of $Cu^+(H_2)_4$, C_s-1; H–H and Cu–H_2 bond lengths are given in pm. (b) CCSD(T)/def2-TZVPP global minimum-energy structure and low-energy saddle point structures of $Cu^+(H_2)_4$ and their electronic energies. See Fig. S2 (ESI†) for different views of these structures. (c and d) Sketch of paths along the potential energy surface of $Cu^+(H_2)_4$. (c) the far H_2 (dark blue) rotates (almost) freely such that any of the near H_2 can be parallel (light blue) to the far H_2. (d) *via* a transition structure with C_{2v} symmetry, the far H_2 (saturated blue) and the near H_2 parallel to it (light blue) can interchange roles (pseudorotation).

3.2 Energetics and PES

The global minimum-energy structure on the CCSD(T)/def2-TVZPP Born–Oppenheimer potential energy surface of $Cu^+(H_2)_4$ is shown in Fig. 2a. All four H_2 molecules coordinate side-on. There is one H_2, which is substantially farther away from the Cu^+ center (183 pm) than the other three (one at 175 pm and two at 177 pm), and which we therefore refer to as the "far H_2". We refer to this structure as C_s-1 since there is exactly one H_2 in the mirror plane. The far H_2 rotates almost freely about the Cu–H_2 axis, as shown in Fig. 2c, with C_s-1 being a local minimum and C_s-0 a first-order saddle point only 2 cm^{-1} higher in energy (see Fig. 2b); other than that, Cu^+–H_2 distances and angles are very similar (see Table S1, ESI†). The energetically next-higher, second-order saddle point (+13 cm^{-1}) is C_{2v}-2 that connects two C_s-0 transition structures as shown in Fig. 2d. In C_{2v}-2, there are two pairs of equivalent H_2 molecules – of which the pair in the mirror plane (175 pm) is closer to the Cu^+ center than the other one (181 pm). The third-order saddle point structure D_{2d}-0 and the fourth-order saddle point structure D_{2d}-4 (see Fig. 2b) are again minimally higher in energy, predicted 25 cm and 35 cm^{-1}, respectively, above C_s-1. D_{2d}-4 was reported as the minimum-energy structure in previous studies.[17] In all structures discussed above, the H–H bond length is approximately 3 pm longer than in free H_2; it ranges from 76.6 pm (far H_2 in C_s structures) to 77.4 pm (near H_2 in C_s structures) and increases with decreasing Cu–H_2 distance.

Two higher-order saddle point structures with D_{4h} symmetry (see Fig. S3, ESI†) are conceivable: D_{4h}-4h, a completely planar structure in which the H_2 molecules lie in the σ_h plane, and

D_{4h}-4v, where they are rotated by 90° and lie in σ_v planes. D_{4h}-4v and D_{4h}-4h are predicted 44 and 46 kJ mol^{-1}, respectively, above C_s-1, *i.e.* substantially above the predicted BDE, D_0 for removal of a H_2 molecules from $Cu^+(H_2)_4$, 21 kJ mol^{-1}. This CCSD(T)/def2-TZVPP BDE is in reasonable agreement with the experimentally determined BDE of 19 kJ mol^{-1} reported previously.[17] The energy corresponds to a wavenumber of 1800 cm^{-1}, indicating that in our experiments a single IR photon should be sufficient to induce photodissociation.

3.3 IRPD spectroscopy

Fig. 3a shows the IRPD spectrum for $Cu^+(H_2)_4$ from 2500 cm^{-1} to 7300 cm^{-1}. The intense and broad band at 3729 cm^{-1} (labeled a_1 in Fig. 3a) is assigned to the excitation of the fundamental transitions involving the four H_2 stretching vibrations ν_{HH} in agreement with previous studies on metal-cation dihydrogen complexes.[19,20,48] Although the corresponding stretching mode in free H_2 is nominally IR inactive, the metal cation induces a transition moment along the intermolecular metal–dihydrogen bond causing it to gain IR intensity.[20] Three smaller features (a_2–a_4) are observed at 3951, 4413 and 4640 cm^{-1}, which we attribute to the excitations of combination bands of ν_{HH} with the low frequency Cu^+–H_2 modes ω_{CuH_2}, ν^{sym}_{HCuH} and ν^{asym}_{HCuH} (see Table 1). The weak feature at 7160 cm^{-1} (a_5) corresponds to the first overtone excitations of the ν_{HH} modes, indicating substantial anharmonicity considering the corresponding fundamental at 3729 cm^{-1}. All observed IRPD bands in the $Cu^+(H_2)_4$ spectrum are wider than 60 cm^{-1}, much broader than the spectral bandwidth of the IR laser pulse (3.5 cm^{-1}). This could arise from rotational band contours, but band profile simulations predict considerably narrower and more structured bands (see Fig. S4 in the ESI†). Moreover, we also measured temperature-dependent IRPD spectra for $Cu^+(H_2)_4$ at trap temperatures of 10 K, 20 K, 35 K and 60 K (see Fig. S4, ESI†). Their analysis further supports that there is a band broadening mechanism present that goes beyond the thermal population of rovibrational levels. Therefore, we attribute the observed band broadening to dynamic effects (see below), *i.e.* large-amplitude motions of the hydrogen molecules that affect ν_{HH}, similar to the situation in the $H_3^+(H_2)_n$ complexes.[49–51]

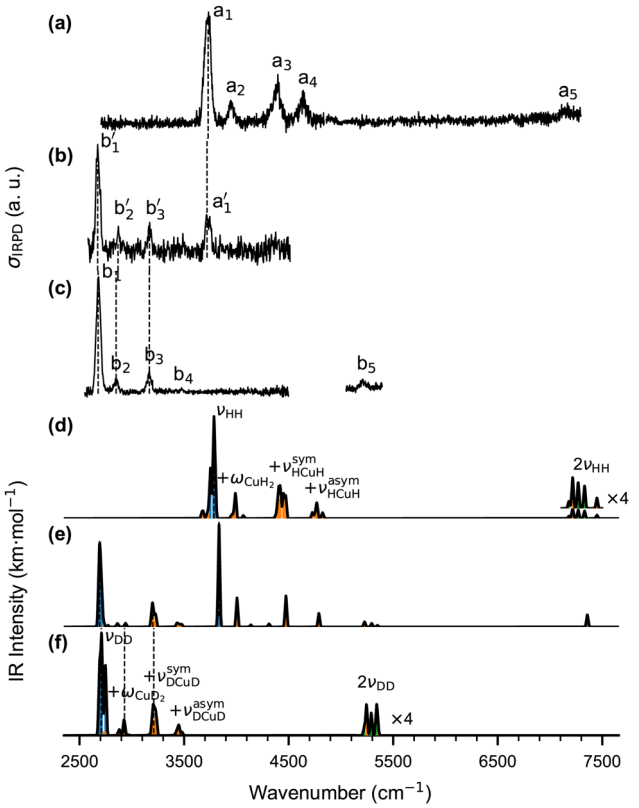

Fig. 3 Comparison of the IRPD spectra of (a) $Cu^+(H_2)_4$, (b) $Cu^+(D_2)_3H_2$ and (c) $Cu^+(D_2)_4$ to the corresponding DVPT2/MP2/def-TZVPP IR spectra of (d) $Cu^+(H_2)_4$, (e) $Cu^+(D_2)_3H_2$ and (f) $Cu^+(D_2)_4$. Band positions and assignments to fundamental (blue), combination (orange) and overtone (green) transitions are listed in Table 1.

The spectrum for the all-D complex $Cu^+(D_2)_4$ (shown in Fig. 3c) looks similar to the all-H spectrum. The main feature in the IRPD spectrum of $Cu^+(D_2)_4$ is centered at 2678 cm^{-1} (b_1). The observed frequency ratio of band a_1 (all-H) *vs.* b_1 (all-D) is 1.39, which is smaller than the ratio calculated from reduced masses of two H_2 isotopologues 1.41 ($\sqrt{\mu_{D_2}-\mu_{H_2}}$), but the same as the ratio of experimental vibrational frequencies for free H_2 (4162 cm^{-1}) and D_2 (2994 cm^{-1}), indicating that the discrepancy is due to anharmonicity. Three weaker bands are found at 2850 (b_2), 3183 (b_3), and 3476 cm^{-1} (b_4). The frequency ratios of the corresponding bands a_2/b_2, a_3/b_3 and a_4/b_4 are 1.39, 1.38 and 1.34, respectively, similar to or smaller than the a_1/b_1 ratio, in agreement with the assumption that these bands originate from combination bands involving low-frequency metal–D_2 modes. The band at 5209 cm^{-1} (b_5) is assigned to the first overtone excitation of ν_{DD}. The observed b_5/a_5 ratio is 1.38, the same as the ratio determined from the first overtone excitations in the neutral dihydrogen isotopologues H_2 (8087 cm^{-1}) and D_2 (5868 cm^{-1}).[52]

The IRPD spectrum of $Cu^+(D_2)_3H_2$, measured by monitoring both H_2 loss ($Cu^+(D_2)_3$ fragment) and D_2 loss ($Cu^+(D_2)_2H_2$ fragment) dissociation channels, is shown in Fig. 3b. Two bands corresponding to the excitation of the ν_{DD} (b_1', 2674 cm^{-1}) and the ν_{HH} (a_1', 3716 cm^{-1}) fundamentals are observed with an intensity ratio of roughly 3 : 1, as could be naively expected. The two remaining features at 2871 cm^{-1} (b_2') and 3169 cm^{-1} (b_3') are then tentatively assigned to the excitation of combination bands involving the ν_{DD} stretching mode (see Fig. 3c). The IRPD spectrum obtained by exclusively monitoring the H_2 loss channel ($Cu^+(D_2)_3H_2 \rightarrow Cu^+(D_2)_3 + H_2$, Fig. S5, in red, ESI†) shows similar bands, but with different intensity, indicating a non-statistical dissociation process. In particular, the relative intensity of band a_1', corresponding to excitation of ν_{HH}, is substantially enhanced compared to the intensity of the bands involving ν_{DD} excitation, *i.e.* bands b_1', b_2' and b_3'.

3.4 VPT2 IR spectra

The DVPT2/MP2/def-TZVPP IR spectra, which we refer to as VPT2 IR spectra from here on, of the global minimum-energy

Table 1 Experimental IR band positions (in cm^{-1}), DVPT2/MP2/def2-TZVPP vibrational frequencies and intensities (in km mol^{-1}, in parenthesis) and band assignments for IR active vibrational modes (> 0.5 km mol^{-1})

Band	Expt.	Calc.	Assignment[a]
$Cu^+(H_2)_4$			
a_1	3729	3800(4), 3790(12), 3781(18), 3751(13)	ν_{HH}
a_2	3951	3993(1), 3991(6), 3971(1), 3952(1)	$\nu_{HH} + \omega_{CuH_2}$
a_3	4413	4472(6), 4450(6), 4423(3), 4418(5), 4403(5), 4399(2), 4375(1), 4390(1)	$\nu_{HH} + \nu^{sym}_{HCuH}$
a_4	4640	4824(2), 4772(1), 4751(1), 4727(2), 4768(3)	$\nu_{HH} + \nu^{asym}_{HCuH}$
a_5	7160	7269 (2), 7180 (1)	$2\nu_{HH}$
		7216 (3)	$\nu_{HH} + \nu_{HH}$
$Cu^+(D_2)_4$			
b_1	2678	2748 (10), 2713 (3), 2710 (13), 2691 (11)	ν_{DD}
b_2	2850	2925 (2)	$\nu_{DD} + \omega_{CuD_2}$
b_3	3183	3236 (2), 3223 (2), 3218 (1), 3206 (2), 3203 (2), 3192 (1)	$\nu_{DD} + \nu^{sym}_{DCuD}$
b_4	3476	3480(1), 3454(1), 3448(1), 3428(1)	$\nu_{DD} + \nu^{asym}_{DCuD}$
b_5	5209	5290 (1), 5222 (0)	$2\nu_{DD}$
		5245 (1)	$\nu_{DD} + \nu_{DD}$
$Cu^+(D_2)_3H_2$			
b_1'	2674	2714 (3), 2698 (11), 2686 (10)	ν_{DD}
b_2'	2871	2883 (0), 2865 (0), 2857 (0)	$\nu_{DD} + \omega_{CuD_2}$
b_3'	3169	3227 (2), 3209 (1), 3201 (2), 3196 (2), 3188 (1)	$\nu_{DD} + \nu^{sym}_{DCuD}$
a_1'	3716	3834 (20)	ν_{HH}

[a] ν: stretching mode, ν^{sym}: symmetric stretching mode, ν^{asym}: antisymmetric stretching mode, ω: wagging mode.

structures of $Cu^+(H_2)_4$, $Cu^+(D_2)_3H_2$, and $Cu^+(D_2)_4$, are shown in Fig. 3d–f and band assignments to particular vibrational modes are listed in Table 1. For $Cu^+(H_2)_4$ and $Cu^+(D_2)_4$, they show satisfactory agreement with the experimental IRPD spectra, confirming the tentative assignments made above. Bands a_2 to a_4 (b_2 to b_4) are indeed combination bands involving the stretching modes ν_{HH} (ν_{DD}) with the Cu–dihydrogen wagging modes ω_{CuH_2} (ω_{CuD_2}), the symmetric H–Cu–H stretching modes ν^{sym}_{HCuH} (ν^{sym}_{DCuD}), and the antisymmetric H–Cu–H stretching modes ν^{asym}_{HCuH} (ν^{asym}_{DCuD}), respectively. Band a_5 (b_5) corresponds to the overtone excitation $2\nu_{HH}$ ($2\nu_{DD}$) yielding a harmonic vibrational frequency term ω_e of 4027 cm^{-1} (2825 cm^{-1}) and an anharmonicity constant $\omega_e\chi_e$ of 149 cm^{-1} (74 cm^{-1}), assuming a simple Morse potential. Hence the $\omega_e(H_2)/\omega_e(D_2)$ ratio is indeed 1.41, the same as the ratio calculated from the reduced masses of the free H_2 isotopologues.

In contrast to the all-H and all-D complexes, the relative isotopomer contribution needs to be considered for $Cu^+(D_2)_3H_2$. The lowest-energy structure of $Cu^+(D_2)_3H_2$ has three isotopomers, one for each of the unique positions of H_2, and the corresponding VPT2 IR spectra are shown in Fig. S6 (ESI†). Of these three isomers, the one where H_2 occupies the far position, is lowest in energy and its spectrum is shown in Fig. 3e. The other isotopomers are predicted less than 1 kJ mol^{-1} higher in energy and hence are expected to also contribute to the IR signal. The positions of the fundamental and combination bands in the IRPD spectrum of $Cu^+(D_2)_3H_2$ are reproduced satisfactorily. However, the predicted relative band intensities, in particular those of transitions involving excitation of ν_{HH}, are overestimated.

3.5 Born–Oppenheimer molecular dynamics (BOMD) simulations

In light of the shallow PES, BOMD simulations were conducted to study the dynamic behavior of the dihydrogen ligands in $Cu^+(H_2)_4$, and $Cu^+(D_2)_4$, and $Cu^+(D_2)_3H_2$. The distribution of Cu–H_2 distances in $Cu^+(H_2)_4$ at different MD temperatures is shown in Fig. 4 (see also Fig. S7, ESI† for the correlation with H–H bond lengths). At an MD temperature of 15 K, two distinct Cu–H_2 distance regimes are found: ≈168 pm and ≈178 pm with corresponding H–H bond lengths of ≈78 pm and ≈77 pm, respectively. Analysis of the BOMD trajectory at 15 K (see Fig. S8a, ESI†) reveals that, most of the time, one

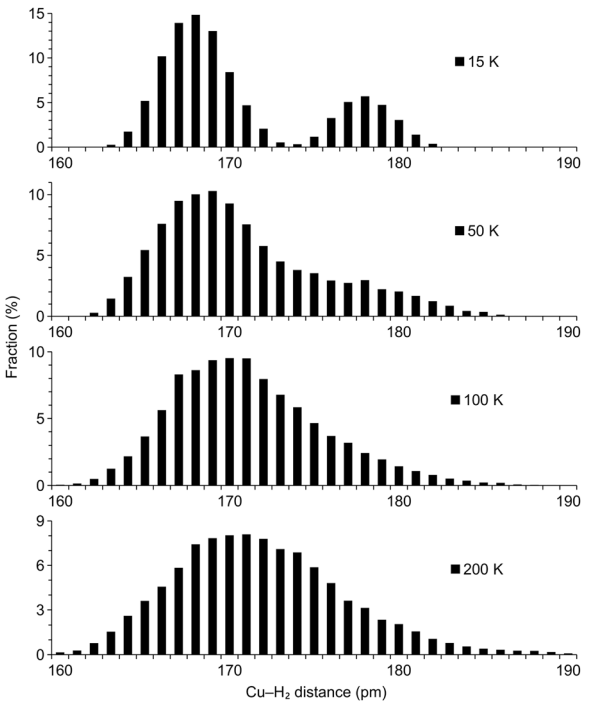

Fig. 4 Histograms of the Cu–H_2 distance (in pm) in $Cu^+(H_2)_4$ at different BOMD temperatures.

H_2 is in the higher-distance regime (far H_2) and the other three are in the lower-distance regime (near H_2). The H_2 molecules can interchange positions *via* pseudorotation on a time scale of the order of 10 ps. At an elevated BOMD temperature of 50 K, the intermediate region between the two maxima is increasingly explored and at 100 K the two regimes merge completely and only a single, much broader maximum centered at 171 pm is found. Furthermore, the Cu–H_2 and H–H distances span much broader ranges at higher temperatures, indicating profound fluxionality. These parameters show a similar temperature dependence for the two other isotopologues, $Cu^+(D_2)_4$ and $Cu^+(D_2)_3H_2$.

3.6 BOMD IR spectra

The dipole moments calculated along the BOMD trajectories are used to obtain the vibrational spectra *via* Fourier transformation of the autocorrelation function of the dipole moment. The resulting BOMD IR spectra are shown in Fig. 5 (and Fig. S9, ESI†). The BOMD IR spectrum of $Cu^+(H_2)_4$ at 15 K (Fig. 5a) shows sharp features and two distinct peaks in the ν_{HH} stretching region. Weak $\nu_{HH} + \nu_{HCuH}$ combination bands are predicted around 4400 cm^{-1} and 4750 cm^{-1}. Increasing the BOMD temperature has several marked effects. First, the spectral features become broader and less distinct at 100 K (Fig. 5a) and even more so at 200 K (Fig. 5a). This suggests that the H_2 molecules increasingly explore the intermediate region between ''near'' and ''far'', as already suggested above (see Fig. 4), and the H–H distance adapts accordingly (see Fig S7, ESI†). Consequently, broader vibrational frequency ranges for both, the high frequency and the low-frequency modes, contributing to the combination bands are explored, which translates directly into broader bands. Second, the relative IR intensity of the combination bands increases with increasing BOMD temperature. The BOMD IR spectra of $Cu^+(D_2)_4$ (Fig. S9, ESI†) and of $Cu^+(D_2)_3H_2$ (Fig. 5b) at different temperatures show the same trends as discussed above for $Cu^+(H_2)_4$. Interestingly, the relative band intensities of the ν_{DD} *vs.* the ν_{HH} fundamental excitation in Fig. 5b is now better reproduced than by the ''static'' VPT2 IR spectrum shown in Fig. 3e and Fig. S6 (ESI†).

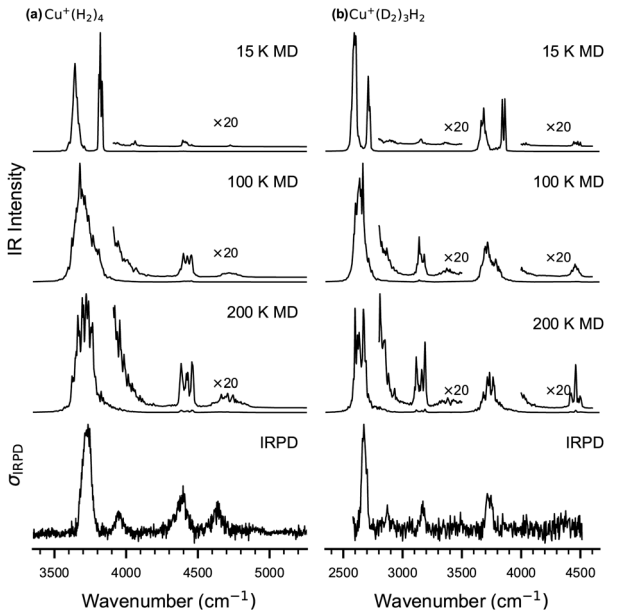

Fig. 5 Comparison of experimental and calculated vibrational spectra of (a) $Cu^+(H_2)_4$ and of (b) $Cu^+(D_2)_3H_2$: BOMD IR spectra at 15 K, 100 K and 200 K (all scaled by 0.932), and experimental IRPD spectrum.

3.7 Thermodynamic properties

According to the VPT2 calculations, anharmonic contributions add up to a total of 6 kJ mol^{-1} for the ZPE of $Cu^+(D_2)_3(H_2)$ – a value much higher than what would be expected based on the values of 0.23 kJ mol^{-1} and 0.12 kJ mol^{-1} for free H_2 and D_2, respectively. Unlike for many systems previously studied, this even translates into a strong effect for the ZPE of the isotopologue exchange reactions. The reaction ZPE of the conversion $Cu^+(D_2)_3(H_2) + D_2 \rightarrow Cu^+(D_2)_4 + H_2$ is −2.7 kJ mol^{-1} according to the harmonic approximation, but only −0.6 kJ mol^{-1} according to VPT2. This demonstrates that anharmonic effects play a profound role in this system. However, similar as for the harmonic approximation, we caution against taking the VPT2 result at face value. While VPT2 does consider anharmonicity and thereby explains the vibrational spectra quite well, it does not capture dynamic effects, which likely affect the thermodynamic properties of the system. Furthermore, entropy effects and therefore Gibbs energies cannot be properly accounted for at this level of theory.

4 Discussion

The broad vibrational bands of $Cu^+(H_2)_4$, $Cu^+(D_2)_4$, and $Cu^+(D_2)_3H_2$ – which are an order of magnitude larger than the intrinsic resolution of the method – cannot be explained based on a model that combines the C_s-1 local minimum structure with internal rotations of the H_2/D_2 molecules (see also the simulation of the rovibrational lines in Fig. S4, ESI†). A careful examination of the potential energy surface of the system reveals a plausible explanation for the broad vibrational bands: $Cu^+(H_2)_4$ and its isotopologues adopt a tetrahedral coordination of the ligands around the central atom. At the same time, the H_2 ligand – when binding to an undercoordinated metal cation – prefers a side-on coordination, resulting in a two-fold rotational axis. The irreconcilability of these two symmetry aspects leads to a situation with only one distinct local minimum structure, C_s-1. However, due its low symmetry, there are 192 equivalent arrangements: four possible positions of the far H_2, three possible locations of the near H_2 perpendicular to it and 2^4 equivalent rotations of the H_2 molecules. Combined with the low-lying transition states C_s-0 and C_{2v}-2 (0.02 and 0.15 kJ mol^{-1}, respectively), this apparently results in a highly fluxional system, which in turn leads to the broadening of vibrational bands observed in the experiment.

This connection between fluxionality and spectral broadening is consistent with other ions (*e.g.* CH_5^+), where the broad

features in the vibrational spectra result from the large-amplitude motion of the internal rotation and flip motions between the numerous equivalent global minima on the PES.[53–55] The low-resolution vibrational spectra of the CH_5^+ cation show a very broad feature for the C–H bending vibrations in the far-IR range as well as the C–H stretching vibrations in mid-IR range.[53,56] Thousands of lines in the C–H stretch region were later resolved and attributed to nuclear spin isomers of CH_5^+ as well as the transitions from different quantum numbers.[54] We attribute the broadening of the bands associated with ν_{HH} to the dynamic behavior of the H_2 molecules, similar to the recently reported broadening of the low-frequency combination band in the IRPD spectrum of Cl^-–H_2.[57] Such a broad and rotationally non-resolved ν_{HH} band is also found in F^-–H_2, where it was attributed to the short life time of the excited predissociation state.[58]

The different IRPD spectra obtained based on the H_2 and D_2 loss channels for $Cu^+(D_2)_3H_2$ suggest that intramolecular vibrational relaxation is incomplete, *i.e.* ergodicity is not achieved on the photodissociation time scale and perturbed by the pseudorotations. The energy deposited initially in the H_2 oscillator preferentially leads to rupture of the Cu^+–(H_2) rather than a Cu^+–(D_2) bond.

Evidence of fluxionality is also found in the spectra derived from BOMD trajectories, especially for the higher simulation temperatures of 50 K and 100 K. Although a relatively rigid geometry is predicted at 15 K, we expect that, in reality, the time scale of the pseudorotation should be shorter and the fluxionality more pronounced when taking nuclear quantum effects (including tunneling) into consideration. While we find it remarkable that VPT2, which is a static method, reproduces the experimental spectra of $Cu^+(H_2)_4$ and $Cu^+(D_2)_4$ as well as it does, the agreement between experimental IRPD and VPT2 spectra is less convincing for the $Cu^+(D_2)_3H_2$ isotopologue. This remains true even when accounting for the contributions of its different isotopomers.

Note, the nuclear spin isomers resulting from *ortho*- and *para*-dihydrogen were recently reported to play an important role in the formation and the far-IR spectroscopy of Cl^-–(H_2) and CN^-–(H_2) anion complexes.[21,22,57] However, the present study focuses on the near-IR spectral region and the positions of rovibrational lines from corresponding nuclear spin isomers are expected to differ by only 0.5 cm^{-1}, *i.e.*, much smaller than the bandwidth of the IR laser pulses of $\sim$3.5 cm^{-1}.

The prominent anharmonicity strongly affects the thermodynamic properties of the system. This has to be considered when making statements involving the ZPE of this system. However, the pronounced effect of anharmonicity on the ZPE of isotopologue exchange reactions predicted by VPT2 is unexpected. Even if genuine, it is likely an idiosyncrasy of the present system, which limits its applicability as a model system for dihydrogen isotopologue separation in general.

5 Conclusions

We have studied the vibrational spectra of the copper cation dihydrogen complexes $Cu^+(H_2)_4$, $Cu^+(D_2)_4$ and $Cu^+(D_2)_3H_2$ by IRPD spectroscopy and high-level theoretical calculations. $Cu^+(H_2)_4$ lacks a highly symmetrical structure that reconciles the tetrahedral coordination with the two-fold rotational axis of the side-on coordinated H_2 ligands. This results in a multitude of equivalent minimum-energy structures. In combination with a shallow potential energy surface, this leads to high fluxionality, manifesting itself in very board features in the vibrational spectrum. The afforded vibrational features are assigned to excitations of H–H stretching fundamentals ν_{HH}, combination bands and ν_{HH} overtones of a minimum-energy structure with C_s symmetry. $Cu^+(D_2)_3H_2$ is found to have two fragmentation channels, yielding different spectra, demonstrating non-ergodic dynamic behavior. The calculated PES indicates that the barriers for pseudorotation are less than 10 cm^{-1}, far below the ZPE. Hence, the vibrational ground state wavefunctions are delocalized and the four H_2 molecules are apparently indistinguishable. Pseudorotation in $Cu^+(D_2)_3H_2$ is also studied using *ab initio* BOMD simulations, which confirm the fluxional behavior for $Cu^+(D_2)_3H_2$ and reveal an upper limit of $\approx$10 ps for the time scale of H_2/D_2 exchange. The peculiarities that make $Cu(H_2)_4^+$ spectroscopically interesting also complicate a deeper understanding of its thermodynamics and make it unsuitable as a model system for the fundamental understanding of adsorptive H_2 isotopologue separation in general. Future studies should therefore include systems with different ligand spheres involving, *e.g.*, oxygen or nitrogen donor atoms and ideally only one H_2 ligand, as is commonly observed in materials considered for adsorptive H_2 isotopologue separation.

Author contributions

J. J. and T. W. contributed equally. J. J. and M. J. performed the experimental works. J. J. curated the experimental data and analysed the spectral data with DVPT2 simulations. T. W. did the potential energy surface calculations and BOMD simulations. J. J. and T. W. wrote the manuscript and prepared the figures. K. R. A. and T. H. designed the study, coordinated the project, supervised the research, contributed to the data interpretation and revised the manuscript.

Conflicts of interest

There are no conflicts to declare.

Acknowledgements

This work was funded by the Deutsche Forschungsgemeinschaft (DFG), Project ID 443871192, GRK 2721: ''HYDROGEN Isotopes ^{1,2,3}H''. J. J. acknowledges the Alexander von Humboldt-Stiftung for a postdoctoral fellowship. T. W. acknowledges the European Social Fund for a PhD fellowship. T. W. and T. H. thank the Center for Information Services and High Performance Computing (ZIH) at TU Dresden for computational resources.

References

1 R. Muhammad, S. Jee, M. Jung, J. Park, S. G. Kang, K. M. Choi and H. Oh, *J. Am. Chem. Soc.*, 2021, **143**(22), 8232–8236.
2 M. Liu, L. Zhang, M. A. Little, V. Kapil, M. Ceriotti, S. Yang, L. Ding, D. L. Holden, R. Balderas-Xicohténcatl and D. He, *Science*, 2019, **143**(22), 8232–8236.
3 S. A. FitzGerald, C. J. Pierce, J. L. C. Rowsell, E. D. Bloch and J. A. Mason, *J. Am. Chem. Soc.*, 2013, **135**(25), 9458.
4 R. Xiong, L. Zhang, P. Li, W. Luo, T. Tang, B. Ao, G. Sang, C. Chen, X. Yan and J. Chen, *Chem. Eng. J.*, 2020, **391**, 123485.
5 H. Oh and M. Hirscher, *Eur. J. Inorg. Chem.*, 2016, 4278.
6 I. Savchenko, B. Gu, T. Heine, J. Jakowski and S. Garashchuk, *Chem. Phys. Lett.*, 2017, **670**, 64.
7 D. Cao, J. Ren, Y. Gong, H. Huang, X. Fu, M. Chang, X. Chen, C. Xiao, D. Liu, Q. Yang, C. Zhong, S. Peng and Z. Zhang, *J. Mater. Chem. A*, 2020, **8**(13), 6319.
8 M. Wahiduzzaman, C. F. J. Walther and T. Heine, *J. Chem. Phys.*, 2014, **141**(6), 64708.
9 J. Teufel, H. Oh, M. Hirscher, M. Wahiduzzaman, L. Zhechkov, A. Kuc, T. Heine, D. Denysenko and D. Volkmer, *Adv. Mater.*, 2013, **25**(4), 635.
10 I. Weinrauch, I. Savchenko, D. Denysenko, S. M. Souliou, H.-H. Kim, M. Le Tacon, L. L. Daemen, Y. Cheng, A. Mavrandonakis, A. J. Ramirez-Cuesta, D. Volkmer, G. Schütz, M. Hirscher and T. Heine, *Nat. Commun.*, 2017, **8**(1), 14496.
11 K. R. Asmis, A. Fielicke, G. von Helden and G. Meijer, Vibrational spectroscopy of gas-phase clusters and complexes, ed. D. Woodruff, In *Atomic clusters: From gas phase to deposited. The chemical physics of solid surfaces*, Elsevier, Amsterdam, Boston, 1st edn, 2007, vol. 12, pp. 327–375.
12 E. J. Bieske and O. Dopfer, *Chem. Rev.*, 2000, **100**(11), 3963.
13 J. M. Lisy, *Int. Rev. Phys. Chem.*, 1997, **16**(3), 267.
14 M. A. Duncan, *Int. Rev. Phys. Chem.*, 2003, **22**(2), 407.
15 K. R. Asmis, M. Brümmer, C. Kaposta, G. Santambrogio, G. von Helden, G. Meijer, K. Rademann and L. Wöste, *Phys. Chem. Chem. Phys.*, 2002, **4**(7), 1101.
16 N. Heine and K. R. Asmis, *Int. Rev. Phys. Chem.*, 2015, **34**(1), 1.
17 P. R. Kemper, P. Weis, M. T. Bowers and P. Maitre, *J. Am. Chem. Soc.*, 1998, **120**(51), 13494.
18 P. Kozyra and W. Piskorz, *Phys. Chem. Chem. Phys.*, 2016, **18**(18), 12592.
19 V. Dryza and E. J. Bieske, *Int. Rev. Phys. Chem.*, 2013, **32**(4), 559.
20 V. Dryza, B. L. J. Poad and E. J. Bieske, *Phys. Chem. Chem. Phys.*, 2012, **14**(43), 14954.
21 F. Dahlmann, C. Lochmann, A. N. Marimuthu, M. Lara-Moreno, T. Stoecklin, P. Halvick, M. Raoult, O. Dulieu, R. Wild and S. Schlemmer, *J. Chem. Phys.*, 2021, **155**(24), 241101.
22 F. Dahlmann, P. Jusko, M. Lara-Moreno, P. Halvick, A. N. Marimuthu, T. Michaelsen, R. Wild, K. Geistlinger, S. Schlemmer and T. Stoecklin, *Mol. Phys.*, 2022, e2085204.
23 A. A. Buchachenko, T. A. Grinev, J. Kłos, E. J. Bieske, M. M. Szczęśniak and G. Chałasiński, *J. Chem. Phys.*, 2003, **119**(24), 12931.
24 S. L. Bragg, J. W. Brault and W. H. Smith, *Astrophys. J.*, 1982, **263**, 999.
25 G. J. Kubas, *J. Org. Chem.*, 2014, **751**, 33.
26 X. Wang, L. Andrews, L. Manceron and C. Marsden, *J. Phys. Chem. A*, 2003, **107**(41), 8492.
27 D. J. Frohman, G. S. Grubbs, Z. Yu and S. E. Novick, *Inorg. Chem.*, 2013, **52**(2), 816.
28 D. G. Artiukhin, E. J. Bieske and A. A. Buchachenko, *J. Phys. Chem. A*, 2016, **120**(27), 5006.
29 N. Heine and K. R. Asmis, *Int. Rev. Phys. Chem.*, 2016, **35**(3), 507.
30 M. Mayer and K. R. Asmis, *J. Phys. Chem. A*, 2021, **125**(14), 2801.
31 M. Brümmer, C. Kaposta, G. Santambrogio and K. R. Asmis, *J. Chem. Phys.*, 2003, **119**(24), 12700.
32 D. J. Goebbert, T. Wende, R. Bergmann, G. Meijer and K. R. Asmis, *J. Phys. Chem. A*, 2009, **113**(20), 5874.
33 W. R. Bosenberg and D. R. Guyer, *J. Opt. Soc. Am. B*, 1993, **10**(9), 1716.
34 J. A. Pople, M. Head-Gordon and K. Raghavachari, *J. Chem. Phys.*, 1987, **87**(10), 5968.
35 G. D. Purvis and R. J. Bartlett, *J. Chem. Phys.*, 1982, **76**(4), 1910.
36 M. J. Frisch, G. W. Trucks, H. B. Schlegel, G. E. Scuseria, M. A. Robb, J. R. Cheeseman, G. Scalmani, V. Barone, B. Mennucci, G. A. Petersson, H. Nakatsuji, M. Caricato, X. Li, H. P. Hratchian, A. F. Izmaylov, J. Bloino, G. Zheng, J. L. Sonnenberg, M. Hada, M. Ehara, K. Toyota, R. Fukuda, J. Hasegawa, M. Ishida, T. Nakajima, Y. Honda, O. Kitao, H. Nakai, T. Vreven, J. A. Montgomery Jr., J. E. Peralta, F. Ogliaro, M. Bearpark, J. J. Heyd, E. N. Brothers, K. N. Kudin, V. N. Staroverov, T. Keith, R. Kobayashi, J. Normand, K. Raghavachari, A. Rendell, J. C. Burant, S. S. Iyengar, J. Tomasi, M. Cossi, N. Rega, J. M. Millam, M. Klene, J. E. Knox, J. B. Cross, V. Bakken, C. Adamo, J. Jaramillo, R. Gomperts, R. E. Stratmann, O. Yazyev, A. J. Austin, R. Cammi, C. Pomelli, J. W. Ochterski, R. L. Martin, K. Morokuma, V. G. Zakrzewski, G. A. Voth, P. Salvador, J. J. Dannenberg, S. Dapprich, A. D. Daniels, O. Farkas, J. B. Foresman, J. V. Ortiz, J. Cioslowski and D. J. Fox, *Gaussian 09*, 2009.
37 F. Weigend and R. Ahlrichs, *Phys. Chem. Chem. Phys.*, 2005, **7**(18), 3297.
38 C. Møller and M. S. Plesset, *Phys. Rev.*, 1934, **46**(7), 618.
39 M. Head-Gordon and T. Head-Gordon, *Chem. Phys. Lett.*, 1994, **220**(1–2), 122.
40 M. J. Frisch, M. Head-Gordon and J. A. Pople, *Chem. Phys. Lett.*, 1990, **166**(3), 275.
41 M. Head-Gordon, J. A. Pople and M. J. Frisch, *Chem. Phys. Lett.*, 1988, **153**(6), 503.
42 V. Barone, *J. Chem. Phys.*, 2005, **122**(1), 14108.
43 M. J. Frisch, G. W. Trucks, H. B. Schlegel, G. E. Scuseria, M. A. Robb, J. R. Cheeseman, G. Scalmani, V. Barone, G. A. Petersson, H. Nakatsuji, X. Li, M. Caricato, A. V. Marenich, J. Bloino, B. G. Janesko, R. Gomperts, B. Mennucci, H. P. Hratchian, J. V. Ortiz, A. F. Izmaylov, J. L. Sonnenberg, D. Williams-Young, F. Ding, F. Lipparini, F. Egidi, J. Goings, B. Peng, A. Petrone, T. Henderson, D. Ranasinghe, V. G. Zakrzewski, J. Gao, N. Rega, G. Zheng,

W. Liang, M. Hada, M. Ehara, K. Toyota, R. Fukuda, J. Hasegawa, M. Ishida, T. Nakajima, Y. Honda, O. Kitao, H. Nakai, T. Vreven, K. Throssell, J. A. Montgomery Jr., J. E. Peralta, F. Ogliaro, M. J. Bearpark, J. J. Heyd, E. N. Brothers, K. N. Kudin, V. N. Staroverov, T. A. Keith, R. Kobayashi, J. Normand, K. Raghavachari, A. P. Rendell, J. C. Burant, S. S. Iyengar, J. Tomasi, M. Cossi, J. M. Millam, M. Klene, C. Adamo, R. Cammi, J. W. Ochterski, R. L. Martin, K. Morokuma, O. Farkas, J. B. Foresman and D. J. Fox, *Gaussian 16*, 2016.

44 C. M. Western, PGOPHER, a Program for Simulating Rotational Structure, University of Bristol, **https://pgopher.chm.bris.ac.uk**.

45 C. M. Western, *J. Quant. Spectrosc. Radiat. Transfer*, 2017, **186**, 221.

46 F. Neese, *Wiley Interdiscip. Rev.: Comput. Mol. Sci.*, 2012, **2**(1), 73.

47 M. Thomas, M. Brehm, R. Fligg, P. Vöhringer and B. Kirchner, *Phys. Chem. Chem. Phys.*, 2013, **15**(18), 6608.

48 C. Emmeluth, B. L. J. Poad, C. D. Thompson, G. H. Weddle and E. J. Bieske, *J. Chem. Phys.*, 2007, **126**(20), 204309.

49 M. A. Boyer, C. S. Chiu, D. C. McDonald, J. P. Wagner, J. E. Colley, D. S. Orr, M. A. Duncan and A. B. McCoy, *J. Phys. Chem. A*, 2020, **124**(22), 4427.

50 T. C. Cheng, L. Jiang, K. R. Asmis, Y. Wang, J. M. Bowman, A. M. Ricks and M. A. Duncan, *J. Phys. Chem. Lett.*, 2012, **3**(21), 3160.

51 T. C. Cheng, B. Bandyopadyay, Y. Wang, S. Carter, B. J. Braams, J. M. Bowman and M. A. Duncan, *J. Phys. Chem. Lett.*, 2010, **1**(4), 758.

52 D. K. Veirs and G. M. Rosenblatt, *J. Mol. Spectrosc.*, 1987, **121**(2), 401.

53 O. Asvany, P. Padma Kumar, B. Redlich, I. Hegemann, S. Schlemmer and D. Marx, *Science*, 2005, **309**(5738), 1219.

54 O. Asvany, K. M. T. Yamada, S. Brünken, A. Potapov and S. Schlemmer, *Science*, 2015, **347**(6228), 1346.

55 X. Huang, A. B. McCoy, J. M. Bowman, L. M. Johnson, C. Savage, F. Dong and D. J. Nesbitt, *Science*, 2006, **311**(5757), 60.

56 E. T. White, J. Tang and T. Oka, *Science*, 1999, **284**(5411), 135.

57 S. Spieler, D. F. Dinu, P. Jusko, B. Bastian, M. Simpson, M. Podewitz, K. R. Liedl, S. Schlemmer, S. Brünken and R. Wester, *J. Chem. Phys.*, 2018, **149**(17), 174310.

58 D. A. Wild, R. L. Wilson, Z. M. Loh and E. J. Bieske, *Chem. Phys. Lett.*, 2004, **393**(4–6), 517.

